

ML-QLS: Multilevel Quantum Layout Synthesis

Wan-Hsuan Lin

wanhsuanlin@ucla.edu

University of California, Los Angeles

USA

Jason Cong

cong@cs.ucla.edu

University of California, Los Angeles

USA

ABSTRACT

Quantum Layout Synthesis (QLS) plays a crucial role in optimizing quantum circuit execution on physical quantum devices. As we enter the era where quantum computers have hundreds of qubits, we are faced with scalability issues using optimal approaches and degrading heuristic methods' performance due to the lack of global optimization. To this end, we introduce a hybrid design that obtains the much improved solution for the heuristic method utilizing the multilevel framework, which is an effective methodology to solve large-scale problems in VLSI design. In this paper, we present ML-QLS, the first multilevel quantum layout tool with a scalable refinement operation integrated with novel cost functions and clustering strategies. Our clustering provides valuable insights into generating a proper problem approximation for quantum circuits and devices. Our experimental results demonstrate that ML-QLS can scale up to problems involving hundreds of qubits and achieve a remarkable 52% performance improvement over leading heuristic QLS tools for large circuits, which underscores the effectiveness of multilevel frameworks in quantum applications.

1 INTRODUCTION

Quantum computing has attracted immense research interest due to its exponential speedup for classical intractable problems. Among various qubit technologies, superconducting qubits are one of the most promising platforms to realize large-scale quantum computing [1, 2, 4]. Within superconducting quantum processors, qubit connectivity is limited, meaning not all pairs of physical qubits are capable of performing a two-qubit gate. However, in the circuit, two-qubit gates can occur between any pair of program qubits. To overcome the connectivity limitation, quantum layout synthesis (QLS) accommodates circuit connectivity to the hardware by introducing additional gates.

As the quantum processor is subject to noise, the solution quality of QLS is an important factor for the circuit performance. First, with short coherence time, qubits will lose information without computation. Thus, minimizing circuit depth is crucial to ensure successful information retrieval. Second, since gate operations are not perfect, additional gates introduced by QLS may exacerbate errors and prolong the circuit execution time. Therefore, to utilize the full computation power of the quantum device, we should minimize the number of extra gates and circuit depth during QLS.

QLS has been proven to be NP-hard [44, 48]. Many heuristic tools are proposed [18, 20, 23–25, 28, 31, 35, 37, 40, 42, 44–46, 52, 55, 56] to solve the problem efficiently. Researchers have been working on developing exact QLS tools [5, 33, 36, 38, 47, 49–51, 53]. These exact approaches often cast QLS problems into constraint programming problems and rely on existing solvers to yield solutions. Comparing the solution quality between the leading heuristic tool Sabre [31] and exact tool OLSQ2 [33], Sabre has a 6-7 \times optimality gap, while

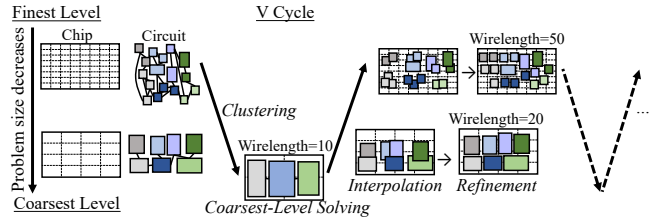


Figure 1: A multilevel V cycle for circuit placement. The inputs to circuit placement are a chip (a transparent box with black boundary) to place objects and a circuit consisting of placeable objects (colored boxes) and nets defining the connection between the objects. The process initiates with iterative clustering to reduce the problem size, continuing until reaching the coarsest level where the problem is directly solved. The placeable objects marked in the same types of color form a coarser object at the coarser level. The dotted lines in chip represents the resolution at the current level. Subsequently, interpolation and refinement are used at each finer level, ultimately yielding the finest-level solution. The dotted lines indicate the possibility of conducting multiple V cycles.

OLSQ2 takes more than one day to compile a size with 36 qubits and 54 gates [15]. As the leading heuristic tools exhibit large optimality gaps and the exact tools struggle with scalability, the demand for scalable and effective QLS tools has been greater in an era of quantum processors with hundreds of qubits [21].

To overcome the scalability issue while keeping a good solution quality, we introduces a novel multilevel framework to harness the strengths of both exact and heuristic approaches. By employing an exact method at the coarsest level for its optimality and integrating scalable heuristics for refinement guided by the optimal coarser solution, we aim to create a hybrid solution that achieves superior performance across a wide range of quantum circuits.

Multilevel frameworks have demonstrated remarkable efficacy in managing large-scale optimization problems across various domains. For example, they are applied in very large-scale integration (VLSI) design, e.g., circuit partitioning [3, 16], placement [6–10, 12, 12, 29], and routing [17, 27, 32, 34, 41], to deal with millions of transistors. Figure 1 shows an example of a multilevel framework for circuit placement.

In this context, the multilevel framework emerges as a powerful tool by constructing a hierarchical problem structure through *clustering* to accelerate the exploration of the solution space at coarser levels. Ideally, the common approach is to group neighboring solutions at finer levels into a unified representation at coarser levels. At the coarsest level, the problem can be solved optimally, often employing solver-based methods, to identify a promising region for further exploration. Although this stage might require a longer runtime, the investment is justified due to the valuable guidance it provides for the following refinement stages.

When transitioning to a finer level, *interpolation* is performed to project a coarser-level solution to the finer-level solution space through declustering. Then, to enhance the solution at the current level, *refinement* is applied to explore the neighboring solution space by leveraging information obtained from the coarser level. This strategy enables efficient exploration of the search space even when the problem size is large. In addition, a multilevel framework can adopt various multilevel flows. For example, after the first V cycle is finished in Figure 1, one can proceed to the second V cycle indicated by the dotted lines. The integration of multiple V cycles plays a crucial role in enhancing the solution’s overall quality by allowing for the iterative refinement of clustering decisions.

In this paper, we present ML-QLS, which is the first work to apply a multilevel framework to provide high-quality results for large-scale quantum circuits. Although a multilevel framework is a well-studied approach in many domains, adopting a multilevel framework to solve QLS is nontrivial due to the unique properties of the QLS problem. We provide an analysis of the challenges and the solutions to effectively address these issues. Our contribution can be summarized as follows:

- We propose ML-QLS, which is the first work to design a multilevel framework tailored specifically for QLS problem.
- We offer a clustering method to effectively construct problem approximations by generating device clustering via the guidance of circuit clustering.
- We propose a heuristic tool, sRefine, which serves as both the standalone layout synthesizer to provide an initial solution and the refinement operation in the multilevel flow. sRefine demonstrates a notable performance improvement by integrating a qubit interaction cost term which is overlooked by previous works.
- ML-QLS reveals its effectiveness with 60% SWAP reduction compared to the leading heuristic QLS tool.

This paper introduces the multilevel framework to the quantum community, showcasing significant performance improvements in QLS and highlighting its potential applicability to a broader range of challenges in quantum computing design automation, e.g., qubit frequency calibration and compilation for other qubit platforms. Through our comprehensive evaluation, we demonstrate that ML-QLS not only addresses the scalability issue but also maintains high solution quality, marking a significant advancement in this field.

2 QUANTUM LAYOUT SYNTHESIS

QLS is a process to map gates in a quantum circuit to a quantum processor defined by a coupling graph and transform circuit connectivity via inserting SWAP gates. The terminology for the inputs is defined as follows.

Quantum circuit: A quantum circuit is defined by a sequence of gates with their target program qubits. In this paper, we denote the set of program qubits by Q , the set of single-qubit gates by G_1 , the set of two-qubit gates by G_2 , and the overall gate set by $G = G_1 \cup G_2$. In addition, we refer to a gate on qubit q and q' by $g(q, q')$. Figure 2(a) depicts a quantum circuit, where each horizontal line is a program qubit, H gates are single-qubit gates, and CNOT gates are two-qubit gates.

Coupling graph: A coupling graph (P, E) defines the connections between physical qubits. Each physical qubit is a vertex $p \in P$, and two physical qubits p, p' can perform a two-qubit gate only if they are the endpoints of an edge. In this paper, an edge between p and p' is denoted by $e(p, p')$. Additionally, we define a distance function $d : P \times P \rightarrow \mathbb{N}$, which is the distance of two physical qubits on the graph. Figure 2(b) illustrates a coupling graph of IBM Ourense [1].

The output to the QLS problem consists of a mapping from program qubits to physical qubits, a gate schedule to indicate the gate execution time, and a list of inserted SWAP. Figure 2(c) shows a valid QLS result using one SWAP to map the circuit in Figure 2(a) to IBM Ourense. The physical location of a program qubit is indicated by the symbol next to the qubit line. For example, program qubit q_0 is mapped to physical qubit p_3 .

Due to the limited connectivity, one fixed mapping may not enable all gate execution. Thus, SWAP gates are inserted into the circuit to adjust qubit mapping. Having additional gates harms the circuit fidelity due to imperfect gate operations. Thus, the objective of QLS is to minimize the number of inserted SWAP gates. Here, we introduce the concept of blocks, where the qubit mapping remains the same. For example, Figure 2(c) consists of two blocks.

A valid QLS result should satisfy the following constraints:

- (1) Mapping injectivity: At any time step, each program qubit should be mapped to a distinct physical qubit.
- (2) Gate dependency: Non-commutable gates should be executed in order if they operate on the same qubits. For example, in Figure 2(a), since g_0 appears before g_4 in the gate sequence and they both act on qubit q_0 , g_0 should be executed before g_4 . On the other hand, for circuits whose gates are commutable, the gates can be executed in any order.
- (3) Valid two-qubit gate execution: To execute a two-qubit gate, its target program qubits should be mapped to adjacent physical qubits. For instance, in Figure 2(c), g_4 can be executed because its target qubits q_0 and q_2 is mapped to an adjacent pair of physical qubits p_3 and p_2 .
- (4) SWAP transformation: The mapping transformation should be consistent with SWAP insertion. In Figure 2(c), initially, q_0 is mapped to p_3 and q_1 is mapped to p_1 . After the SWAP gate occurs, q_0 is mapped to p_1 , and q_1 is mapped to p_3 .

3 MULTILEVEL QUANTUM LAYOUT SYNTHESIS

In this section, we offer a multilevel QLS tool, ML-QLS, consisting of two stages: initial QLS solution construction, followed by the multilevel V cycle. Both stages provide a QLS solution. Figure 3 illustrates our overall workflow. We first discuss the challenges of applying a multilevel framework to solve a QLS problem and our solutions in Section 3.1. Then, in Section 3.2 to Section 3.3, we detail our clustering and the coarsest-level solving techniques. In Section 3.4, we present sRefine, which is our scalable refinement algorithm and can serve as a standalone QLS tool in the first stage.

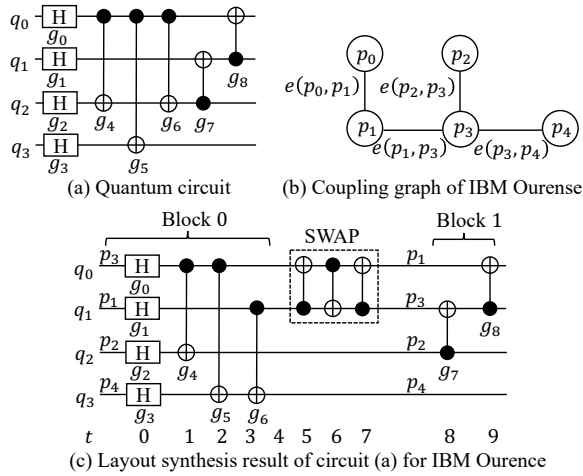


Figure 2: An example of a quantum circuit, coupling graph, and the corresponding QLS result.

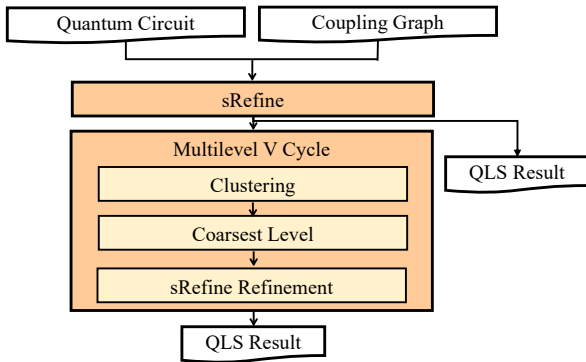


Figure 3: ML-QLS flow.

3.1 Multilevel Framework for QLS

Although the multilevel method is intuitive and well-developed in other domains, there are multiple challenges when integrating it into a QLS tool.

3.1.1 Challenge 1 – Difficulty in device clustering. One of the primary challenges in QLS arises from the nontrivial device clustering. In traditional multilevel frameworks, clustering is typically applied independently to one problem input, such as the graph in graph partitioning or the circuit objects in circuit placement. Even with the need to cluster the input device, i.e., chip, in circuit placement or routing, the device clustering is trivial by applying different granularity to a chip. For example, a chip with a dimension of 100×100 can form a coarser chip with a dimension of 50×50 by adjusting the unit grid length. The trivial device clustering in circuit placement does not alter the solution space because the coarser chips preserve the properties of the finest chip, such as the chip shape or the relative distance between points. Therefore, the cost at the coarser level can serve as a good indicator of the finer-level result.

However, in QLS, clustering an input quantum device and circuit independently results in suboptimal final results because, for an input device, there are many clustering options to form coarser devices, and different coarser devices define varied solution spaces. Given a coupling graph, we have different options to construct

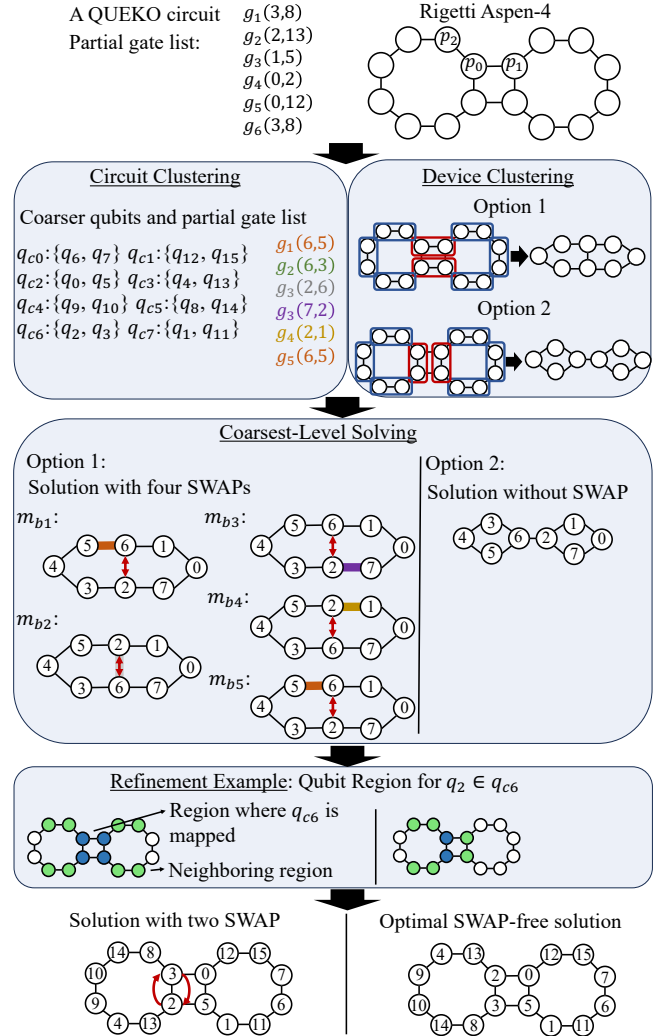


Figure 4: A V cycle example for a QUEKO circuit and Rigetti Aspen-4 coupling graph to demonstrate the effect of clustering on the final QLS solution. The partial gate list of the QUEKO circuit is shown at the top of the figure. A proper circuit clustering is given, including coarser qubits with finer qubits and the coarser partial gate list. For device clustering, we may have two options to generate different coarser coupling graphs. At the coarsest level, the first option leads to an optimal solution with four SWAP gates, while we get a SWAP-free solution with the second clustering option. m_{bi} denotes the mapping for an edge in block i is marked by a thick line in m_{bi} using the same color for font in the coarser partial gate list. The edges for SWAP gates are indicated by red double arrow lines. With the coarsest-level solution, we show the qubit region for q_2 as a refinement example. After refinement, we obtain a solution using two and zero SWAP gates with the first and second clustering options, respectively.

coarser physical qubits, which leads to distinct coarser coupling graphs. For instance, Figure 4 illustrates two clustering options to construct coarser devices for Rigetti Aspen-4. The two coarser devices have distinct connectivity, and none of them has the same topology as Rigetti Aspen-4. Unlike device clustering in VLSI design, device clustering in QLS can not preserve the properties of

the original device such as the topology. Additionally, the relative distance between two physical qubits changes as well. In Rigetti Aspen-4, the distance between p_0, p_2 and p_0, p_1 is one, while the distance between p_1, p_2 is two. However, for the coarser device with clustering option 1, the distance between p_0, p_2 remains one, but the distance between p_0, p_1 is changed to zero, and p_1, p_2 is changed to one. On the other hand, if we apply clustering option 2, the distance between those qubits remains the same. The relative distance change for qubits is unwanted as it alters the solution space by favoring certain QLS results. As shown in Figure 4, the optimal solutions at the coarsest level are inconsistent in terms of both SWAP count and qubit mapping with different device clustering, leading to different final QLS results after refinement.

In this example, option 2 is a better device clustering strategy as it produces solutions with lower SWAP count compared to option 1 at every stage. According to the final QLS result from clustering option 2, we note that the circuit clustering is consistent with the device clustering. That is, the physical qubits are clustered iff the program qubits mapped to them are clustered. Therefore, we propose a strategy that integrates information from both the device and the circuit to ensure harmonious alignment between them. Drawing inspiration from multilevel flow with multiple V cycles, our clustering decisions are guided by a good solution obtained from our heuristic QLS tool, sRefine. For circuit clustering, we tend to cluster program qubits that have many two-qubit gate interactions and are mapped to adjacent physical qubits to take into account the physical information. Then, the device clustering is derived based on circuit clustering and the QLS solution to ensure that device clustering decisions are informed by circuit information.

3.1.2 Challenge 2 – Hidden cost within cluster. Clustering plays a pivotal role in generating problem approximations within the multilevel framework as the cost within a cluster is often overlooked. For example, in circuit placement, the wirelength of placeable objects within a cluster can not be observed at the coarse level. Therefore, when we transit from a coarser level to a finer level, the cost often increases rather than decreases as shown in Figure 1. As the cost increase is hard to estimate, selecting an optimal solution at a coarser level for the later finer level is difficult. QLS has the hidden cost problem as circuit placement as well because the cost of gate execution within a physical qubit cluster is zero. Thus, the challenge lies in selecting an appropriate clustering strategy that effectively represents the original problem at coarser levels.

In QLS, the size of clusters is a crucial factor in cost estimation. While larger cluster sizes may reduce the number of levels in the cycle, they can introduce inaccuracies during the coarsest-level solving or refinement stages. In the context of program qubit clustering, we often cluster qubits that interact frequently, as these clusters remain physically close during circuit execution. However, when choosing larger cluster sizes, a challenge emerges: Not all pairs of physical qubits within a cluster share direct connections, necessitating the insertion of hidden SWAP gates. This can lead to imprecise SWAP cost estimation, impacting solution selection during each stage. To address this, our clusters contain only two physical qubits to ensure zero-cost gate execution within each cluster.

3.1.3 Challenge 3 – Discrete solution space. Discrete solution space of QLS poses a significant challenge for interpolation and refinement. For mathematical optimization problems where solutions transit smoothly from one level to another, people can easily project a coarser-level solution to the finer-level solution space by interpolation. Then, the derived solution is the starting point for the refinement operation in the current stage. In circuit placement, people can decide the location of objects based on the location of their corresponding coarser-level objects as depicted in Figure 1 and gradually adjust the object location to reduce wirelength. However, QLS involves discrete decisions such as qubit mapping, gate scheduling, and SWAP operations, making it impossible to directly derive an initial QLS solution based on a coarser-level solution.

For refinement, one of the challenges originates from the difficulty of recognizing a promising coarser-level solution for the finer level. First, as we are not able to derive an initial solution via interpolation, the cost change between levels is unpredictable. Thus, selecting a good coarser-level solution that can lead to a better finer-level solution is hard. Second, minor changes in the coarse-level solution can lead to vastly different outcomes at the finer level, making it difficult to predict how optimizations will propagate across levels.

As the coarser-level solution may not be optimal for the finer-level problem, selecting useful information from the coarser-level solution to guide the finer-level solving becomes crucial during the refinement stage. In a multilevel framework, refinement operations are expected to perform local optimization and are encouraged not to excessively alter the initial solution from interpolation because the initial solution is globally optimized. For example, in circuit placement, one common strategy is to add a term to minimize the objective displacement to the initial solution. Nevertheless, we cannot obtain an initial solution in our case.

In our framework, we propose the concept of *mapping regions*, which are promising solution regions suggested by the coarser-level solving. For each program qubit q , a mapping region R_q is defined as follows: First, the physical qubits where q is mapped are included in R_q . Then, to facilitate exploration of neighboring solution spaces, R_q is expanded to encompass physical qubits within a one-hop distance from the mapped qubits. This expansion facilitates a more flexible and efficient exploration of adjacent solution options. In case of misguidance from suboptimal solutions, our refinement operation encourages qubits to stay within their mapping regions but not restrict them, allowing for greater adaptability in the optimization process. Figure 4 illustrates the construction of qubit regions, demonstrating how this approach permits effective exploration of neighboring solution spaces.

3.2 Clustering

To create coarser circuits and coupling graphs, we initiate the process by generating coarser program and physical qubits. For program qubits, we can define the affinity between qubit pairs according to the two-qubit gates in the circuit. The affinity between two program qubits will increase for each two-qubit gate acting on them. Next, according to the descending order of affinity values, we iteratively cluster two finer program qubits which are mapped to the adjacent physical qubits based on the solution from sRefine. For those program qubits that remain unclustered after the first run of

clustering, we cluster them based on their initial mapping from the solution of sRefine (to be described in Section 3.5), i.e., cluster two program qubits that are mapped to the adjacent physical qubits.

For the physical qubits, we first collect them based on the corresponding program qubit clustering. For instance, if program qubits q and q' are mapped to physical qubits p and p' respectively, while q and q' form a clustered program qubit, then p and p' will form a clustered physical qubit. Lastly, we iteratively cluster an unclustered physical qubit with its unclustered neighbor or the smallest neighbor cluster. Figure 4(a) and (b) illustrate a clustering example.

For the coarser coupling graph, we bundle physical qubits p_i and p'_i to form a coarser physical qubit p_{c_i} . We establish an edge between p_{c_i} and p_{c_j} if there exists an edge between $p \in \{p_i, p'_i\}$ and $p' \in \{p_j, p'_j\}$.

Regarding the construction of a coarser circuit, for each gate in the original circuit, if it operates on two distinct coarser qubits q_c and q'_c , we include the gate $g(q_c, q'_c)$ in the coarser circuit. Conversely, if a gate operates on the same coarser qubit, we omit it from the circuit, assuming that there is no inherent cost associated with executing a gate within a coarser physical qubit. Since qubit regions are the only information required from the coarser level, we do not introduce gate dependency at the coarser level. In addition, there is a dependency between two gates in the coarser circuit if there is a dependency between the corresponding gates in the finer circuit. We repeatedly generate a coarser problem via clustering until the coarsest-level problem is tractable for TB-OLSQ2.

3.3 Coarsest-Level Optimization

In the coarsest level, TB-OLSQ2 [33] is used to solve the problem. TB-OLSQ2 is the state-of-the-art optimal SMT-based QLS tool and is scalable by adopting the concept of gate blocks. Their SMT formulation consists of three types of variables: (1) mapping variables to represent the mapping from program qubits to physical qubits for each block, (2) gate time variables to encode the block for gate execution, (3) SWAP variables to indicate the use of SWAP gate on each edge between gate blocks, and four types of constraints as discussed in Section 2. Their SWAP optimization is a two-dimensional search along block number and SWAP count to generate Pareto optimal results. In our implementation, we impose a runtime limit of 100 seconds after we obtain the first SWAP optimization results.

According to our experimental results, TB-OLSQ2 can return a solution for problem size with about 20 qubits and 50 gates efficiently. Thus, it can serve as a tool to provide high-quality solutions at the coarsest level for problems less than this threshold.

3.4 Scalable Refinement: sRefine

sRefine has two components: SA-based initial mapping and A*-based SWAP insertion. Section 3.4.1 and 3.4.2 detail the implementation when serving as refinement operations, while Section 3.5 presents the modifications when used as a standalone QLS tool in the first stage.

3.4.1 SA-Based Initial Mapping. In this stage, our primary objective is to establish an initial mapping that facilitates the execution of all gates while minimizing the need for SWAP gates. To achieve

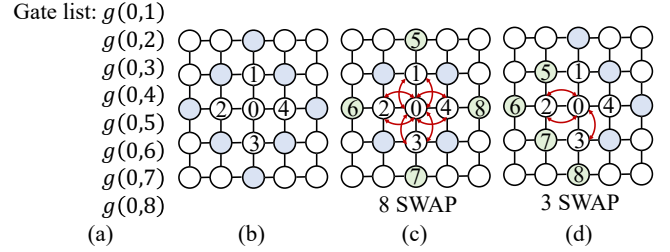


Figure 5: An example to exhibit the effectiveness of $DisForRelatedQubits$. (a) A gate list. (b) Optimal mapping on a grid coupling graph for q_0 to q_4 based on Eq. 2. Placing q_5 to q_8 on any of the blue circles yields the same cost. (c) One optimal solution based on Eq. 2 uses eight SWAP gates. (d) One optimal solution based on Eq. 1 employs three SWAP gates.

this, we define a cost function as follows:

$$Cost(m) = DisForGates(m) + DisForRelatedQubits(m), \quad (1)$$

where $m : Q \rightarrow P$ is the mapping from program qubits to physical qubits. $DisForGates$ in Eq. 1 accounts for the distance between target qubits for two-qubit gates, which is calculated by

$$DisForGates(m) = \sum_{g(q,q') \in G_2} w_g \times d(m(q), m(q')), \quad (2)$$

where w_g is the weight of a gate. To account for the fact that gates farther from the beginning of the circuit should have less influence on the initial mapping decision, w_g decreases exponentially relative to the gate's distance from the beginning of the circuit.

Additionally, it is beneficial to position qubits that interact with the same qubit near each other. This improves the likelihood of sharing SWAP operations. Figure 5 illustrates an example. According to the gate list in Figure 5(a), one optimal mapping for q_0 to q_4 under Eq. 1 is shown in Figure 5(b). Under Eq. 2, mapping q_5 to q_8 to any of the blue circles results in the same optimal cost. Figure 5(c) demonstrates one optimal solution that requires eight SWAP gates. In this example, no SWAP gates can be shared between gates. However, by arranging the qubits that interact with the same qubits nearby, as depicted in Figure 3(d), we only need three SWAP gates, as one SWAP gate is shared by three gates. Thus, we add the novel cost $DisForRelatedQubits$ to capture the distance between related qubits for two consecutive two-qubit gates.

$$DisForRelatedQubits(m) = \sum_{\substack{g \in G_2 \\ g' \in Parent(g)}} w_g \times d(m(q'), m(q'')), \quad (3)$$

where $Parent(g)$ denotes the set of the last two-qubit gates acting on the target qubits of g while q' and q'' represent the uncommon qubits between g and g' . For instance, in Figure 5, $g(0,2) \in Parent(g(0,3))$ because both gates operate on q_0 , and $g(0,2)$ is the last previous two-qubit gate involving q_0 .

During refinement, qubits have a higher chance to move within its qubit region derived from the coarser level solution, and the initial solution for SA is a maximal matching within the bipartite graph $G(V, E)$, where $V = Q \cup P$ and $(q, p) \in E$ if $p \in R_q$. Note that the maximal matching can be obtained by Edmonds' Blossom algorithm in $O(|E||P|^2)$ [19].

Subsequently, we utilize the Fast-SA algorithm [11], which has three stages of temperature modification for efficient solution space exploration, to optimize our cost function. Within the SA-based initial mapping method, each state defines a unique mapping configuration. The neighbors of a state are generated by selecting a qubit and relocating it to a new position. If the chosen location is already occupied by another qubit, we exchange their positions.

3.4.2 A*-Based SWAP Insertion. In contrast to the approach of inserting one SWAP gate at a time, as employed in SABRE [31], we adopt a strategy that selects a set of SWAP gates for a set of gates simultaneously to consider more global information when deciding qubit movement. Consequently, we develop an A*-based algorithm capable of exploring multiple gates concurrently.

To address the state explosion problem inherent in A* search, we design a state trimming mechanism. When the number of states exceeds a predefined threshold s , we retain only the k states with the lowest cost. Empirically, we set $s = 100$ and $k = 50$. In our A* search, a state stands for a qubit mapping and a set of gates waiting for execution. More specifically, a state v consists of five elements:

- An edge e where the SWAP occurs,
- A set of gates G_{ready} ready for execution, i.e., their ancestors are all mapped, but they cannot be executed under the current mapping,
- A set of gates $G_{unexecuted}$ not yet ready for execution,
- Its parent state u
- The cost $f(v) = g(v) + h(v)$, where $g(v)$ is the SWAP cost from the initial state to the current state, and $h(v)$ is an estimated SWAP cost from the current state to the goal state.

When transitioning from a state u to its child state v , we alter the mapping by inserting one SWAP gate. Consequently, we define $g(v_0) = 0$, where v_0 represents the initial state, and $g(v) = g(u) + 1$, where u is the parent state of v .

The heuristic cost $h(v)$ is calculated as follows:

$$\begin{aligned}
 h(v) = & \frac{\sum_{g(q,q') \in G_{ready}} d(m(q), m(q'))}{|G_{ready}| * |Q|} \\
 & + \alpha \times \frac{\sum_{g(q,q') \in G_{oneHopReady}} d(m(q), m(q'))}{|G_{oneHopReady}| * |Q|} \\
 & + \beta \times \frac{\sum_{g'(q,q') \in Parent(g), g \in G_{oneHopReady}} d(m(q), m(q'))}{|G_{oneHopReady}| * |Q|} \\
 & + \gamma \times |G_{unexecuted}|,
 \end{aligned} \tag{4}$$

where $m(q)$ denotes the current mapping of q , and $G_{oneHopReady} = \{g' | g'(q, q') \in Child(g), g \in G_{ready}\}$. α , β , γ are the user-defined hyperparameters. In our implementation, we set $\alpha = \beta = 0.5$ and $\gamma = 0.1$. The first term in the cost depicts the normalized qubit distance cost for the gates in G_{ready} , while the second term serves as the lookahead cost and represents the normalized qubit distance cost for the gates in $G_{oneHopReady}$, with a weight of 0.5. The third term is the normalized cost for the related qubit distance as defined in Eq. 3, and the last term signifies the number of unexecuted gates, indicating the progress of a state. The weight assigned to the last term determines the trade-off between SWAP insertion and gate

execution. A weight of 0.1 signifies that it is worthwhile to insert one SWAP gate for every ten gate executions.

To enhance the efficiency of the search space exploration, we employ several strategies. Firstly, we restrict our consideration to SWAP gates associated with the target qubits of gates in G_{ready} . Second, in alignment with Eq. 4, we encourage target qubits to be moved closer to each other. Consequently, if a SWAP gate would relocate a qubit farther from its target qubit, we opt not to expand the node, thus conserving computational resources. In addition, to follow the guidance from the coarser-level solution, the node associated with a SWAP that moves a qubit out of its qubit region will have a small probability of being expanded.

In this stage, we refine the initial mapping based on routing information by applying the concept of forward and backward compilation passes, as proposed in [31]. The forward pass compiles the original circuit, while the backward pass compiles the reverse circuit. In our framework, we utilize the mapping returned by the SA-based initial mapping as the initial mapping for our first forward pass. Then, the final mapping from the first forward pass serves as the initial mapping for the reverse circuit in the subsequent backward pass. Similarly, the final mapping from the backward pass can be used as the initial mapping for the original circuit in the next forward pass. This iterative process continues until the SWAP count from the current compilation pass is not better than the previous one. The best result obtained thus far is considered our final solution. This approach leverages the interplay between forward and backward compilation passes to iteratively refine the mapping, ultimately yielding an optimized solution.

3.5 Standalone QLS Tool

The standalone QLS tool is a variant of sRefine. First, we do not force the qubit to be in a certain region, there is no restriction for SA movement and node expansion in A* search. Second, when used as a standalone QLS tool, we design InitialMapper to provide a good quality initial solution for the Fast-SA algorithm. InitialMapper is an SMT-based method designed to generate a mapping that enables the execution of most gates within the circuit. Although we can use a random mapping as the initial solution, a high quality starting point can facilitate efficient solution exploration for Fast-SA.

The formulation of InitialMapper is a simplified variant of TB-OLSQ2 by removing time dimension, SWAP, gate time variables and the related constraints. InitialMapper only contains mapping variables $m(q)$ for each qubit and associated mapping constraints. Our approach involves a stepwise addition of gates $g(q, q') \in G_2$ with the constraint

$$\begin{aligned}
 & \bigwedge_{e(p,p') \in E} ((m(q) == p) \wedge (m(q') == p')) \\
 & \vee ((m(q') == p) \wedge (m(q) == p')).
 \end{aligned} \tag{5}$$

This constraint is incorporated into the solver, and the iterative process unfolds as follows: If the instance is proved satisfiable, we proceed to add the subsequent gate following the predefined gate order. Conversely, if the instance turns out unsatisfiable, we remove the constraint associated with the most recently added gate and introduce the constraint for the subsequent gate in line. Throughout this process, we maintain the solution with the lowest cost. The

candidate with the lowest cost is then designated as the initial solution for the SA-based initial mapping.

Regarding the gate order, while one could use the naive order derived from the circuit, such an approach may not maximize the number of executed gates and could favor solutions with fewer SWAP gates at the beginning of the circuit. Therefore, we opt to generate the gate order by shuffling gates randomly to mitigate potential biases toward certain types of solutions.

Since both InitialMapper and the SA-based initial mapping incorporate randomness, we generate five initial mapping candidates for the subsequent SWAP insertion stages to produce layout synthesis solutions. The best among these candidates is selected as the final result. To manage the exponential growth in SMT solving time, we only invoke InitialMapper if the number of program qubits is fewer than 100. Additionally, we impose a runtime limit of 1000 seconds for the first run and 100 seconds for subsequent runs.

4 EVALUATION

In this section, we detail our evaluation methods and the evaluation results.

4.1 Experimental Settings

Benchmark and Baseline. Our benchmark circuits include QUEKO circuits [48], which are used for evaluating layout synthesizers, QAOA [54] phase-splitting operator for random 3-regular graphs with a vertex number ranging from 24 to 300, and circuits from QASMBench [30] with a qubit number ranging from 28 to 280 and a gate number ranging from 42 to 2146. The QAOA circuits are generated by networkx (v2.4) [22]. Note that the gates in QAOA circuits are all commutable.

Our targeting coupling graphs are of two types: grid architectures and heavy-hexagon architectures. For grid architectures, we benchmark against different grid lengths ranging from 5 to 31. and the Google’s Sycamore processor with 54 qubits [4]. In addition, we use IBM’s Eagle processor with 127 qubits [13] to represent the heavy-hexagon architecture. We compare the performance of our tool against the leading heuristic layout synthesizers, Sabre [31] with Qiskit (v1.0.2) implementation.

Experimental Platform. We implemented our proposed algorithm in C++ programming language with Boost C++ libraries [14] and provided a Python interface via PyBind11 [26] for evaluation. We employed the Bitwuzla (v0.4.0) [39] for SMT solving and pplib [43] for cardinality constraint-to-CNF generation. All experiments were conducted on an AMD EPYC 7V13 64-Core Processor at 2450 MHz and 128 GB of RAM.

4.2 Evaluation on QAOA Circuits

Figure 6 and 7 demonstrate SWAP count comparison between SABRE and ML-QLS for QAOA circuits across the Eagle architecture and the grid architectures where the grid length are set to be $\lceil \sqrt{|Q|} \rceil$. For ML-QLS, results from both stages are provided. According to the figure, results returned by the V cycle are better than sRefine. The performance of V cycle is 11% and 18% better than sRefine for the Eagle architecture and grid architectures, respectively. This trend underscores the effectiveness of the multilevel

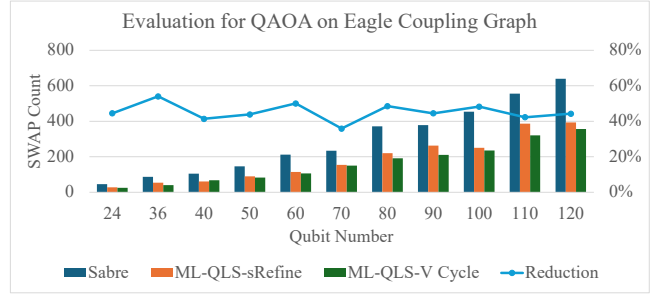


Figure 6: SWAP count comparison for QAOA circuits for random 3-regular graphs of size 24 and 120 on an IBM Eagle coupling graph.

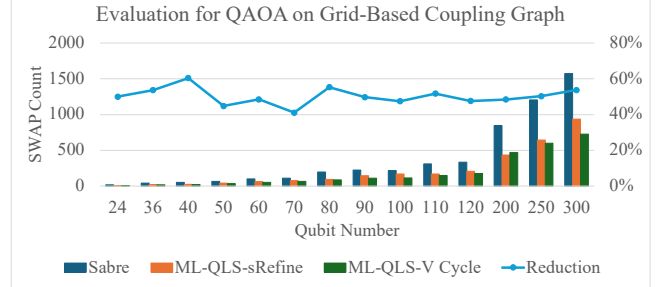


Figure 7: SWAP count comparison for QAOA circuits for random 3-regular graphs of size 24 and 300 on grid-based coupling graphs.

framework, showing that the coarsest-level solution provides good guidance for subsequent refinement for the circuit without gate dependency. In addition, V cycle improves grid architectures better than the Eagle architecture does, and we posit the reason is that the dense connectivity in coupling graphs alleviates the inaccurate cost estimation in the multilevel framework. As discussed in Section 3.1.3, the estimation of the cost increase for coupling graphs with sparse connectivity is difficult since we may not have all-to-all connectivity between coarser qubits. Moreover, comparing the performance gap for sRefine and V cycle on the same architecture, we observe that the gap is enlarged when the problem sizes increase, showing that our multilevel framework is more powerful when dealing with large instances. In summary, ML-QLS achieves an average of 46% improvement with a maximal 60% improvement and a minimal improvement of 36% against Sabre. For the solving time, circuits on grid and Eagle architectures can be completed by ML-QLS within 2 hours and 30 minutes, respectively.

4.3 Evaluation on QASMBench Circuits

The results for circuits from QASMBench benchmark suite on the grid architectures are reported in Figure 8, and the results on the Eagle architecture are shown in Figure 9. In comparison to commutable cases, V cycle exhibits reduced effectiveness in the presence of gate dependencies on both architectures. With the presence of gate dependency, V cycle is 4% better and 7% better than sRefine for Eagle and grid-based coupling graphs, respectively. We observe that V cycle can perform better on the grid architectures, which is in accordance with our observation in Section 4.2. In summary, ML-QLS achieves an average of 50% and 39% SWAP reduction for grid and Eagle architectures, respectively. In terms of scalability, ML-QLS takes an average of 10 minutes to solve the problem.

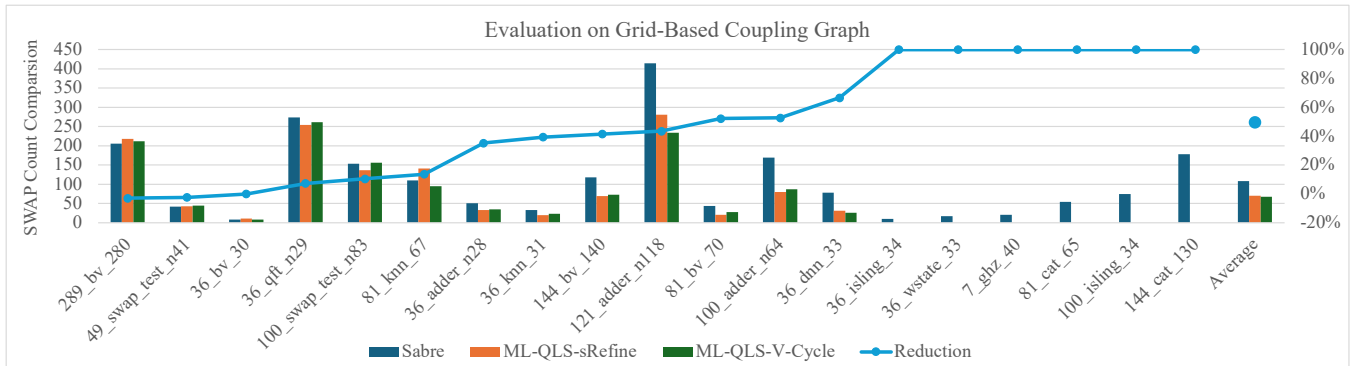


Figure 8: SWAP count comparison for circuits from QASMBench benchmark suites on grid-based coupling graph. The prefix of the benchmark circuit name is the number of physical qubits in the coupling graph, while the suffix denotes the number of program qubits in the circuit. For example, 36_adder_n28 represents the adder circuit with 28 qubits on a 6-by-6 grid coupling graph.

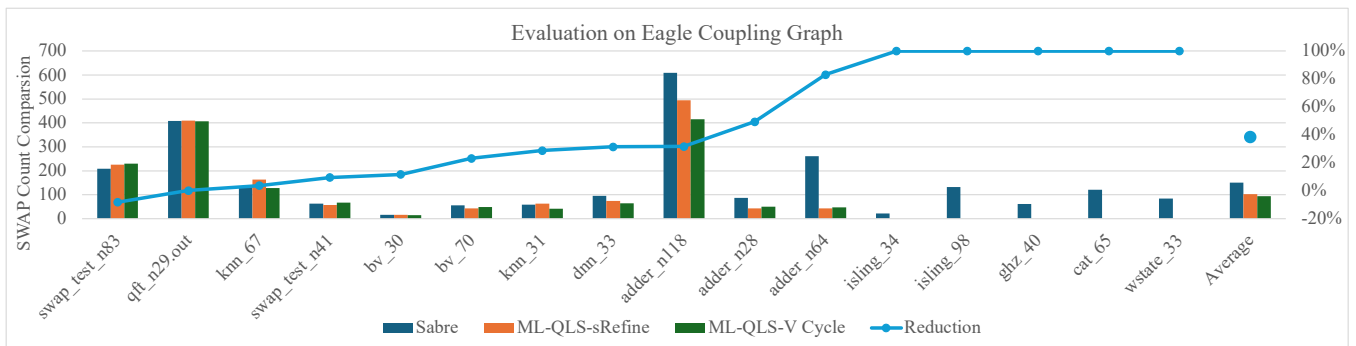


Figure 9: SWAP count comparison for circuits from QASMBench benchmark suites on an IBM Eagle coupling graph.

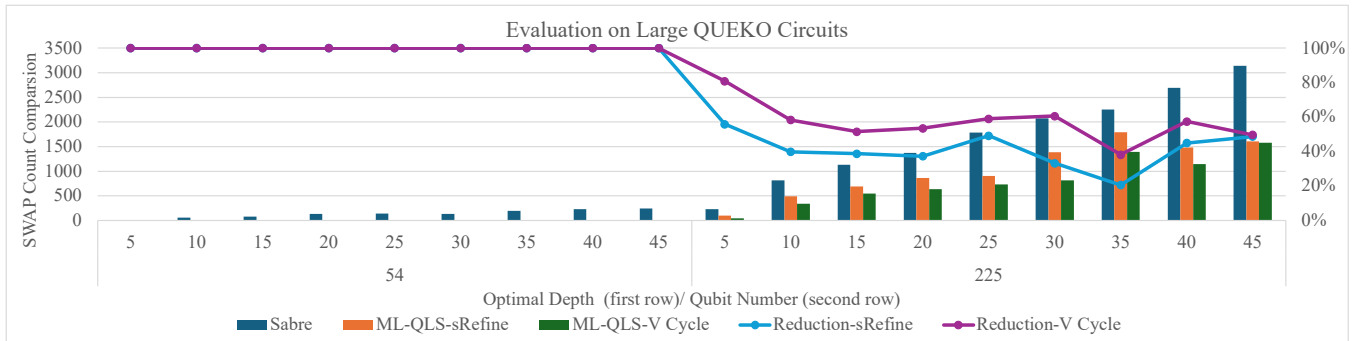


Figure 10: The optimality gap for SABRE and ML-QLS measured by QUEKO circuits with an optimal depth ranging from 5 to 45 for Google Sycamore architecture and a 15-by-15 grid architecture.

4.4 Evaluation on QUEKO Circuits

The evaluation results for QUEKO circuits are demonstrated in Figure 10. In this experiment, we evaluate both methods on QUEKO circuits with an optimal depth ranging from 5 to 45 for Google Sycamore architecture and a 15-by-15 grid architecture. With InitialMapper, our tool can effectively find a SWAP-free mapping and achieve optimal circuit depth for circuits with less than 100 qubits. Thus, we can always obtain the optimal results. On the other hand, due to the randomness and heuristics characteristics in Sabre, those results have an average of 4.7x optimality gap in depth and use 179 SWAP gates per circuit on average. In terms of

the solving time, ML-QLS can return a solution within two minutes for all 54-qubit circuits. For large instances with 225 qubits, we do not invoke InitialMapper due to scalability concern for an SMT solver. According to the figure, V cycle consistently produce higher quality results than sRefine, demonstrating the effectiveness of the multilevel framework. Compared to Sabre, ML-QLS can achieve an average of 57% SWAP reduction. For the compilation time, the circuit with an optimal depth of 45 can take four hours to solve.

5 CONCLUSION

In this paper, we propose the first multilevel quantum layout tool, ML-QLS. This tool includes sRefine, which is an effective heuristic QLS tool that incorporates a novel cost function to capture the SWAP cost, clustering strategy, and efficient refinement. Our experimental results demonstrate that ML-QLS has a 57% performance improvement over the leading heuristic QLS tool for large circuits. ML-QLS showcases the efficacy of multilevel frameworks in quantum applications, offering valuable insights for researchers exploring hierarchical approaches. Its accomplishments highlight the significance of iterative, multilevel strategies in optimizing quantum compilation processes. ML-QLS sets a precedent for advancing quantum layout tools and strategies, paving the way for future developments in quantum computing optimization.

6 ACKNOWLEDGEMENTS

The authors would like to thank Bochen Tan, Jason Kimko, Yunong Shi, Eric Kessler, and Yaroslav Kharkov for useful discussion about quantum layout synthesis and valuable comments on the manuscript. This research is supported in part by the National Science Foundation Award 2313083 and the Amazon under the Science Hub program.

REFERENCES

- [1] [n. d.]. *IBM Quantum*. <https://quantum-computing.ibm.com>
- [2] [n. d.]. *Rigetti Computing*. <https://www.rigetti.com>
- [3] Charles J Alpert et al. 1997. Multilevel circuit partitioning. In *Proceedings of the 34th annual Design Automation Conference*. 530–533.
- [4] Frank Arute et al. 2019. Quantum supremacy using a programmable superconducting processor. *Nature* 574, 7779 (2019), 505–510.
- [5] Debjoyoti Bhattacharjee, Abdullah Ash Saki, Mahabubul Alam, Anupam Chattopadhyay, and Swaroop Ghosh. 2019. MUQUT: Multi-constraint quantum circuit mapping on NISQ computers. In *2019 IEEE/ACM International Conference on Computer-Aided Design*. IEEE, 1–7.
- [6] T.F. Chan et al. 2003. An enhanced multilevel algorithm for circuit placement. In *ICCAD-2003. International Conference on Computer Aided Design (IEEE Cat. No.03CH37486)*. 299–306.
- [7] Tony Chan, Jason Cong, and Kenton Sze. 2005. Multilevel generalized force-directed method for circuit placement. In *Proceedings of the 2005 International Symposium on Physical Design*. 185–192.
- [8] Tony F Chan et al. 2000. Multilevel optimization for large-scale circuit placement. In *IEEE/ACM International Conference on Computer Aided Design. ICCAD-2000. IEEE/ACM Digest of Technical Papers (Cat. No. 00CH37140)*. IEEE, 171–176.
- [9] Tony F Chan et al. 2005. mPL6: A robust multilevel mixed-size placement engine. In *Proceedings of the 2005 International Symposium on Physical Design*. 227–229.
- [10] Tung-Chieh Chen et al. 2005. NTUplace: A ratio partitioning based placement algorithm for large-scale mixed-size designs. In *Proceedings of the 2005 International Symposium on Physical Design*. 236–238.
- [11] Tung-Chieh Chen and Yao-Wen Chang. 2006. Modern floorplanning based on B/sup */-tree and fast simulated annealing. *IEEE Transactions on Computer-Aided Design of Integrated Circuits and Systems* 25, 4 (2006), 637–650. <https://doi.org/10.1109/TCAD.2006.870076>
- [12] Chung-Kuan Cheng et al. 2018. Replace: Advancing solution quality and routability validation in global placement. *IEEE Transactions on Computer-Aided Design of Integrated Circuits and Systems* 38, 9 (2018), 1717–1730.
- [13] Jerry Chow, Oliver Dial, and Jay Gambetta. 2021. IBM Quantum breaks the 100-qubit processor barrier. *IBM Research Blog* (2021).
- [14] Marshall Clow and Glen Fernandes. 2023. *The Boost C++ Libraries*. https://www.boost.org/users/history/version_1_82_0.html
- [15] Jason Cong. 2023. Lightning Talk: Scaling Up Quantum Compilation—Challenges and Opportunities. In *2023 60th ACM/IEEE Design Automation Conference*. IEEE, 1–2.
- [16] Jason Cong and Sung Kyu Lim. 2004. Edge separability-based circuit clustering with application to multilevel circuit partitioning. *IEEE Transactions on Computer-Aided Design of Integrated Circuits and Systems* 23, 3 (2004), 346–357.
- [17] Jason Cong and Yan Zhang. 2005. Thermal-driven multilevel routing for 3-D ICs. In *Proceedings of the 2005 Asia and South Pacific Design Automation Conference*. 121–126.
- [18] Poulami Das et al. 2022. ForeSight: Reducing SWAPs in NISQ Programs via Adaptive Multi-Candidate Evaluations. *arXiv preprint arXiv:2204.13142* (2022).
- [19] Jack Edmonds. 1965. Paths, trees, and flowers. *Canadian Journal of mathematics* 17 (1965), 449–467.
- [20] Hongxiang Fan et al. 2022. Optimizing quantum circuit placement via machine learning. In *Proceedings of the 59th ACM/IEEE Design Automation Conference (San Francisco, California) (DAC '22)*. Association for Computing Machinery, New York, NY, USA, 19–24.
- [21] Jay Gambetta. 2023. The hardware and software for the era of quantum utility is here.
- [22] Aric A. Hagberg et al. 2008. Exploring Network Structure, Dynamics, and Function using NetworkX. In *Proceedings of the 7th Python in Science Conference*. Pasadena, CA USA, 11 – 15.
- [23] Alan Ho and David Bacon. 2018. Announcing Cirq: an open source framework for NISQ algorithms. *Google AI Blog* 18 (2018).
- [24] Ching-Yao Huang et al. 2022. Reinforcement Learning and DEAR Framework for Solving the Qubit Mapping Problem. In *Proceedings of the 41st IEEE/ACM International Conference on Computer-Aided Design*. 1–9.
- [25] IBM. 2018. *Qiskit*. Retrieved 2021-11-21 23:27:25 -0800 from <https://qiskit.org/>
- [26] Wenzel Jakob, Jason Rhinelander, and Dean Moldovan. 2022. pybind11 – Seamless operability between C++11 and Python. <https://github.com/pybind/pybind11>.
- [27] George Karypis, Rajat Aggarwal, Vipin Kumar, and Shashi Shekhar. 1997. Multilevel hypergraph partitioning: Application in VLSI domain. In *Proceedings of the 34th annual Design Automation Conference*. 526–529.
- [28] Abhoy Kole et al. 2020. Improved Mapping of Quantum Circuits to IBM QX Architectures. *IEEE Transactions on Computer-Aided Design of Integrated Circuits and Systems* 39, 10 (Oct. 2020), 2375–2383.
- [29] David Leong and Guy G.F. Lemieux. 2009. Replace: An incremental placement algorithm for field programmable gate arrays. In *2009 International Conference on Field Programmable Logic and Applications*. IEEE, 154–161.
- [30] Ang Li et al. 2022. QASMBench: A Low-Level Quantum Benchmark Suite for NISQ Evaluation and Simulation. *ACM Transactions on Quantum Computing* (2022).
- [31] Gushu Li et al. 2019. Tackling the qubit mapping problem for NISQ-era quantum devices. Association for Computing Machinery, New York, NY, USA, 1001–1014.
- [32] Shih-Ping Lin and Yao-Wen Chang. 2002. A novel framework for multilevel routing considering routability and performance. In *Proceedings of the 2002 IEEE/ACM International Conference on Computer-Aided Design*. 44–50.
- [33] Wan-Hsuan Lin et al. 2023. Scalable optimal layout synthesis for NISQ quantum processors. In *2023 60th ACM/IEEE Design Automation Conference*. IEEE, 1–6.
- [34] Jinwei Liu et al. 2020. CUGR: Detailed-routability-driven 3D global routing with probabilistic resource model. In *2020 57th ACM/IEEE Design Automation Conference (DAC)*. IEEE, 1–6.
- [35] Ji Liu et al. 2022. Not all SWAPs have the same cost: a case for optimization-aware qubit routing. In *2022 IEEE International Symposium on High-Performance Computer Architecture*. 709–725. ISSN: 2378-203X.
- [36] Abtin Molavi et al. 2022. Qubit mapping and routing via MaxSAT. In *2022 55th IEEE/ACM International Symposium on Microarchitecture*. IEEE, 1078–1091.
- [37] Prakash Murali et al. 2019. Formal constraint-based compilation for noisy intermediate-scale quantum systems. *Microprocessors & Microsystems* 66, C (April 2019), 102–112. <https://doi.org/10.1016/j.micpro.2019.02.005>
- [38] Giacomo Nannicini et al. 2022. Optimal qubit assignment and routing via integer programming. *ACM Transactions on Quantum Computing* 4, 1 (2022), 1–31.
- [39] Aina Niemetz and Mathias Preiner. 2023. Bitwuzla. In *Computer Aided Verification - 35th International Conference, 2023, Paris, France, July 17-22, 2023, Proceedings, Part II*, Constantin Enea and Akash Lal (Eds.), Vol. 13965. Springer, 3–17. https://doi.org/10.1007/978-3-031-37703-7_1
- [40] Siyuan Niu et al. 2020. A Hardware-Aware Heuristic for the Qubit Mapping Problem in the NISQ Era. *IEEE Transactions on Quantum Engineering* 1 (2020), 1–14.
- [41] Hung-Chih Ou et al. 2012. Non-uniform multilevel analog routing with matching constraints. In *Proceedings of the 49th Annual Design Automation Conference*. 549–554.
- [42] Sunghye Park et al. 2022. A Fast and Scalable Qubit-Mapping Method for Noisy Intermediate-Scale Quantum Computers. In *Proceedings of the 59th ACM/IEEE Design Automation Conference*. New York, NY, USA, 13–18.
- [43] Tobias Philipp and Peter Steinke. 2015. PBLib – A Library for Encoding Pseudo-Boolean Constraints into CNF. In *Theory and Applications of Satisfiability Testing – SAT 2015*, Marijn Heule and Sean Weaver (Eds.), Vol. 9340. Springer International Publishing, 9–16.
- [44] Marcos Yukio Siraichi et al. 2018. Qubit allocation. Association for Computing Machinery, New York, NY, USA, 113–125. <https://doi.org/10.1145/3168822>
- [45] Marcos Yukio Siraichi et al. 2019. Qubit allocation as a combination of subgraph isomorphism and token swapping. *Proceedings of the ACM on Programming Languages* 3, OOPSLA (Oct. 2019), 120:1–120:29. <https://doi.org/10.1145/3360546>
- [46] Seyon Sivarajah et al. 2020. t|ket>: a retargetable compiler for NISQ devices. *Quantum Science and Technology* 6, 1 (Nov. 2020), 014003. <https://doi.org/10.1098/rsos.200140>

- 1088/2058-9565/ab8e92
- [47] Bochen Tan and Jason Cong. 2020. Optimal layout synthesis for quantum computing. In *Proceedings of the 39th International Conference on Computer-Aided Design*. ACM, 1–9. <https://doi.org/10.1145/3400302.3415620>
 - [48] Bochen Tan and Jason Cong. 2020. Optimality study of existing quantum computing layout synthesis tools. *IEEE Trans. Comput.* 70, 9 (2020), 1363–1373.
 - [49] Bochen Tan and Jason Cong. 2021. Optimal qubit mapping with simultaneous gate absorption. In *2021 IEEE/ACM International Conference On Computer Aided Design*. IEEE, 1–8.
 - [50] Robert Wille et al. 2019. Mapping quantum circuits to IBM QX architectures using the minimal number of SWAP and H operations. In *Proceedings of the 56th Annual Design Automation Conference 2019*. 1–6.
 - [51] Robert Wille, Aaron Lye, and Rolf Drechsler. 2014. Optimal SWAP gate insertion for nearest neighbor quantum circuits. In *2014 19th Asia and South Pacific Design Automation Conference (ASP-DAC)*. IEEE, 489–494.
 - [52] Tsou-An Wu et al. 2022. A Robust Quantum Layout Synthesis Algorithm with a Qubit Mapping Checker. In *Proceedings of the 41st IEEE/ACM International Conference on Computer-Aided Design (ICCAD '22)*. Association for Computing Machinery, New York, NY, USA, Article 105, 9 pages.
 - [53] Chi Zhang and others. 2021. Time-optimal Qubit mapping. Association for Computing Machinery, New York, NY, USA, 360–374.
 - [54] Leo Zhou et al. 2020. Quantum Approximate Optimization Algorithm: Performance, Mechanism, and Implementation on Near-Term Devices. *Physical Review X* 10, 2 (June 2020), 021067. <https://doi.org/10.1103/PhysRevX.10.021067>
 - [55] Alwin Zulehner et al. 2018. An efficient methodology for mapping quantum circuits to the IBM QX architectures. *IEEE Transactions on Computer-Aided Design of Integrated Circuits and Systems* 38, 7 (2018), 1226–1236.
 - [56] Alwin Zulehner et al. 2019. An Efficient Methodology for Mapping Quantum Circuits to the IBM QX Architectures. *IEEE Transactions on Computer-Aided Design of Integrated Circuits and Systems* 38, 7 (July 2019), 1226–1236.